Model biases in the atmosphere-ocean partitioning of poleward heat transport are persistent across three CMIP generations

A. Donohoe[1,3], R. Fajber[2], T. Cox [3], K.C. Armour[3,4], D.S. Battisti [3]and G.H. Roe [4]

[1]Polar Science Center, Applied Physics Laboratory

University of Washington

Seattle, Washington 98195, USA.

[2] Department of Atmospheric and Oceanic Sciences, McGill University

[3] Department of Atmospheric and Oceanic Sciences, University of Washington

[4]School of Oceanography, University of Washington

[5]Department of Earth and Space Sciences, University of Washington

Key Points:

- Climate models simulate too little poleward oceanic heat transport and too much poleward atmospheric heat transport in the extratropics
- Model biases in heat transport partitioning are persistent across model generation and are insensitive to the observational data sets used
- Stronger than observed evaporation in models enhances atmospheric heat transport at the expense of oceanic heat transport

Abstract

The observed partitioning of poleward heat transport between atmospheric and oceanic heat transports (AHT and OHT) is compared to that in coupled climate models. Poleward OHT in the models is biased low in both hemispheres, with the largest biases in the Southern Hemisphere extratropics. Poleward AHT is biased high in the Northern Hemisphere, especially in the vicinity of the peak AHT near 40°N. The significant model biases are persistent across three model generations (CMIP3, CMIP5, CMIP6) and are insensitive to the satellite radiation and atmospheric reanalyses products used to derive observational estimates of AHT and OHT. Model biases in heat transport partitioning are consistent with biases in the spatial structure of energy input to the ocean and atmosphere. Specifically, larger than observed model evaporation in the tropics adds excess energy to the atmosphere that drives enhanced poleward AHT at the expense of weaker OHT.

Plain Language Summary

The equator-to-pole contrast of solar radiation entering the climate system drives the large-scale oceanic and atmospheric circulations that, in turn, move heat from the equator to the poles to moderate latitudinal temperature contrasts. The ocean moves the majority of heat in the tropics whereas the atmosphere moves the vast majority of heat in the mid- and polar-latitudes. We demonstrate that state-of-the-art climate models representing both oceanic and atmospheric circulations systematically simulate too little oceanic heat transport and too much atmospheric heat transport relative to observational estimates. These model biases in the atmosphere-ocean partitioning of poleward heat transport are persistent across three generations of climate model ensembles spanning twenty years of progress in climate modeling and are insensitive to the choice of datasets used to calculate observed heat transports. The model biases are consistent with stronger than observed surface evaporation in the tropics which enhances atmospheric heat transport at the expense of oceanic heat transport.

1 Introduction

The combined meridional heat transport (MHT) by the ocean and atmosphere moderates spatial gradients in temperature on Earth. In the absence of MHT, the equator-to-pole temperature gradient would be approximately three times larger than observed based on radiative considerations alone (Pierrehumbert, 2010), rendering the tropics uninhabitably warm and the high latitudes uninhabitably cold. Observational estimates of the partitioning of MHT between poleward atmospheric heat transport (AHT) and poleward oceanic heat transport (OHT) show that OHT exceeds AHT in the deep tropics (equatorward of 10°) while AHT dominates in the mid- and high-latitudes of both hemispheres (Vonder Haar & Oort, 1973; Oort & Haar, 1976; Trenberth & Caron, 2001; Mayer et al., 2021).

The partitioning of MHT between AHT and OHT impacts climate and its changes. For example, the convergence of OHT in the extratropics is inherently linked to the surface energy budget and thus demands a surface temperature response, whereas the convergence of the same quantity of AHT in the atmosphere can be radiated to space with less impact on surface climate (Cardinale et al., 2020). Indeed, previous work by Enderton & Marshall (2009) has shown that aquaplanets with nearly identical total MHT but different AHT-OHT partitioning can have very different climates (e.g., different surface temperature and sea ice distributions).

Given the dependence of climate on the partitioning between poleward AHT and OHT, we ask here: how well do coupled climate models represent the observed AHT-OHT partitioning? This question was briefly addressed in Chapter 9 of the Intergovern-

⁶⁹ mental Panel on Climate Change 5th assessment report (Flato et al., 2013) which con-
⁷⁰ cluded that model OHT was within the wide range of observational OHT estimates. Com-
⁷¹ parison of observational and model AHT-OHT partitioning is difficult because the stan-
⁷² dard methodology for partitioning MHT between AHT and OHT differs between obser-
⁷³ vations and models due to the contrasting reliability and availability of the climate fields
⁷⁴ used to calculate AHT and OHT. Recent work (Donohoe et al., 2020) has demonstrated
⁷⁵ the near equivalence of the model and observational approaches to AHT-OHT partition-
⁷⁶ ing in a model setting, enabling a comprehensive observational-model comparison. In
⁷⁷ this study we apply these methods to three generations of coupled model simulations (Phases
⁷⁸ 3, 5, and 6 of the Coupled Model Intercomparison Project, CMIP) and to several obser-
⁷⁹ vational radiation and atmospheric reanalysis products. Our aim is to determine whether
⁸⁰ the models accurately capture the partitioning of AHT and OHT derived from obser-
⁸¹ vational datasets.

⁸² In Section 2 we provide an overview of the observational and model methodologies
⁸³ for partitioning MHT into AHT and OHT and demonstrate the near equivalence of these
⁸⁴ two approaches. In section 3, we compare the observational and model MHT partition-
⁸⁵ ing across the three different model generations (CMIP3, CMIP5, and CMIP6) and ex-
⁸⁶ amine the sensitivity of our findings to the choice of observational data sets used to par-
⁸⁷ tition MHT. In Section 4 we consider an alternative method for comparing AHT-OHT
⁸⁸ partitioning in models and observations from the processes that contribute to spatial gra-
⁸⁹ dients in energy input to the atmosphere and ocean. A summary and discussion follows.

2 Methods for partitioning MHT into AHT and OHT in observations and coupled models

⁹² The methodology used to partition MHT into AHT and OHT in coupled climate
⁹³ models and observations is described in detail in Donohoe et al. (2020). Here we sum-
⁹⁴ marize the conceptual approach.

2.1 Heat transport partitioning in climate models

⁹⁶ Near closure of the top of atmosphere (TOA) and surface energy budgets in climate
⁹⁷ models allows for the energy transport by the atmosphere and ocean across a latitude
⁹⁸ band to be calculated from the energy input into/out-of the fluid spatially integrated over
⁹⁹ the polar cap bounded by that latitude:

$$\text{MHT}(\Theta) = 2\pi a^2 \int_{\Theta}^{90} -F^* \cos\theta d\theta, \tag{1}$$

¹⁰⁰ where a is the radius of the Earth, Θ is the latitude (with θ a latitude variable of inte-
¹⁰¹ gration), and F is the net energy input to the atmosphere, ocean, or combined atmosphere-
¹⁰² ocean system. The total MHT can be found by taking F to be the radiative flux at the
¹⁰³ TOA (RAD$_{\text{TOA}}$), OHT by taking F to be the net surface heat flux (SHF = radiative
¹⁰⁴ plus turbulent flux into the ocean), and AHT by setting F to be the net energy input
¹⁰⁵ to the atmosphere (RAD$_{\text{TOA}}$ - SHF). The * denotes that the global mean of each en-
¹⁰⁶ ergy flux term has been removed to ensure heat transport goes to zero at both poles. This
¹⁰⁷ adjustment is necessary because climate models do not conserve energy globally (≈ 1 W
¹⁰⁸ m^{-2} imbalances) in both the atmosphere and ocean (Lucarini & Ragone, 2011).

2.2 Heat transport partitioning in observations

¹¹⁰ In contrast to coupled climate models where the surface energy budget is (nearly)
¹¹¹ closed, the sparsity and uncertainty of observational surface radiative and turbulent en-
¹¹² ergy flux measurements results in an unrealistically large (>10 W m^{-2}) global mean sur-

face energy imbalance (Stephens et al., 2012; Trenberth et al., 2009), which prohibits the evaluation of OHT from the net surface heat flux. Instead, we use a conceptual approach following Vonder Haar & Oort (1973) and Trenberth & Caron (2001): MHT is calculated using Eq. 1 with satellite RAD_{TOA} (Loeb & Coauthors, 2018); AHT is calculated from the time average of the vertically and zonally integrated meridional energy flux in the atmosphere derived from high frequency (6 hourly) atmospheric reanalysis; OHT is then calculated as the residual of satellite derived MHT and reanalysis derived AHT. In the AHT calculation, a vertically integrated moist static energy anomaly is removed before integrating (Donohoe & Battisti, 2013; Cardinale et al., 2020; Donohoe et al., 2020), effectively applying a mass correction needed to make the AHT calculation physically meaningful (Trenberth & Stepaniak, 2003; Liang et al., 2018).

To show that the "observational" and "model" methods are comparable, we partition MHT into AHT and OHT using both methods in a NCAR CESM1 coupled pre-industrial control simulation (see Donohoe et al., 2020, for details). The two approaches give nearly identical partitioning of MHT into AHT and OHT (cf. the dashed and solid red and blue lines in Supporting Information Fig. S1) with a root mean squared difference AHT (and OHT) between the two methods of 0.07 PW. The close correspondence of the two calculations of MHT partitioning suggests that the "observational" and "model" approaches we use here to partition MHT are directly comparable. We use this result to justify the examination of potential model biases in MHT partitioning using these two methodologies.

3 Results: model biases in MHT partitioning

Climate model biases in MHT partitioning are analyzed using pre-industrial control simulations from three different CMIP generations and several different sets of observational products (see Supporting Information for details). The presentation of our results is organized as follows. Section 3.1 presents the observational estimate of MHT partitioning using the most contemporary and high resolution data available, which is compared against the MHT partitioning in the three CMIP ensembles. Section 3.2 analyzes the sensitivity of our results to the observational data used by comparing eight different observational estimates of MHT partitioning against the multi-generation CMIP ensemble mean. The results show that the sign and spatial structure of model biases in MHT partitioning are consistent across model generation and observational data sets used.

3.1 Consistent model biases in AHT-OHT partitioning across three CMIP generations

In this section, we use CERES Energy Balanced and Filled (EBAF) TOA radiation (Loeb et al., 2009) and the ERA5 atmospheric reanalysis (Hersbach et al., 2020) to calculate an observational estimate of MHT and its partitioning over the period 2001-2020. This observational estimate (solid line) is compared against each of the three CMIP ensembles (in each row of Fig. 1; with dashed lines showing individual models and the thick dashed lines showing CMIP ensemble averages).

Poleward MHT peaks near $35°$ in both hemispheres in both models and observations (Fig. 1), consistent with constraints due to Earth-Sun geometry whereby the meridional distribution of net TOA radiation (RAD_{TOA}^*) is dominated by the second order Legendre polynomial (equator-to-pole scale) as discussed by Stone (1978). However, across all three CMIP generations, the amplitude of poleward MHT in models is biased low in the mid-latitudes of both hemispheres relative to the observational estimate. In the Southern Hemisphere (SH), the observational estimate of maximum poleward MHT is 5.7 PW, which is significantly larger (95% confidence interval of t-test) than the ensemble means of CMIP3 (5.2 PW), CMIP5 (5.3 PW), and CMIP6 (5.4 PW). In the Northern Hemisphere (NH) the observational estimate of maximum poleward MHT is 5.8 PW, exceed-

163 ing the ensemble mean of CMIP3 (5.6 PW), CMIP5 (5.5 PW), and CMIP6 (5.7 PW),
164 but only for CMIP5 is the difference statistically significant. In the SH, the inter-model
165 spread in peak MHT (2 standard deviations) is as large as 23% of the ensemble mean
166 and has values of 1.2 PW in CMIP3, 0.8 PW in CMIP5, and 0.8 PW in CMIP6. The
167 inter-model spread in peak NH MHT is smaller than its SH counterpart with values of
168 0.8 PW in CMIP3, 0.6 PW in CMIP5, and 0.6 PW in CMIP6. Donohoe & Battisti (2011)
169 demonstrated that the the inter-model spread and bias in MHT in CMIP3 results from
170 biases and spread in the albedo of clouds which impact the equator-to-pole gradient of
171 absorbed solar radiation. The bias and spread in MHT is only slightly reduced in CMIP5
172 and CMIP6, and also results primarily from model differences in mean-state shortwave
173 cloud radiative effects (not shown).

174   We next analyze the partitioning of MHT between OHT and AHT. In the NH, the
175 model ensemble mean is significantly biased toward too little poleward OHT and too much
176 poleward AHT in all three CMIP generations. The observational estimate of peak NH
177 AHT is 4.4 PW as compared to 4.7 ± 0.2 PW in CMIP3, 4.7 ± 0.1 PW in CMIP5, and
178 4.8 ± 0.1 PW in CMIP6 where the stated uncertainty is two standard deviations of the
179 ensemble mean. The peak in NH OHT is robustly equatorward of the peak AHT, but
180 has significantly larger values for the observational estimate (2.0 PW) than in the model
181 ensemble means (1.7 PW in CMIP3, 1.8 PW in CMIP5, and 1.7 PW in CMIP6). The
182 model bias toward smaller than observed OHT extends poleward to the Arctic where OHT
183 has been demonstrated to have large impacts on sea ice extent (Holland et al., 2006; Sea-
184 ger et al., 2002).

185   In the SH, poleward OHT in the models is biased low relative to the observational
186 estimate in all three CMIP generations. The largest biases in OHT are found the vicin-
187 ity of 40°S where the observational OHT is -0.7 PW compared to the ensemble mean
188 OHT at that latitude is -0.3 ± 0.2 PW in CMIP3, -0.2 ± 0.1 PW in CMIP5, and -0.1
189 ± 0.1 PW in CMIP6. The observational estimate of poleward OHT is only exceeded in
190 three model simulations (two in CMIP3 and one in CMIP5). In contrast, the poleward
191 AHT in the SH is not significantly different between the models and observational es-
192 timates.

193   These results suggest that in the SH, the majority of the model biases in MHT are
194 a result in biases in OHT, whereas in the NH the models generally simulate too much
195 poleward AHT and too little poleward OHT. Alternatively, the fractional contribution
196 of AHT-OHT to total MHT (i.e., normalizing each model by the model specific MHT)
197 is biased toward too much poleward AHT and too little poleward OHT with biases that
198 are nearly hemispherically symmetric between the two hemispheres (not shown). Impor-
199 tantly, the sign and spatial structure of model biases in MHT and AHT-OHT partition-
200 ing are remarkably consistent across the three CMIP generations spanning over 20 years
201 of progress in climate modeling.

3.2 Sensitivity of results to observational data sets used

203   We next consider whether the identified model biases in AHT-OHT partitioning
204 are sensitive to the choice of observational data sets (TOA radiation and atmospheric
205 reanalysis) used to partition MHT. We use the mean of all ensemble members across all
206 three CMIP generations, referred to as the CMIP-mean, as a reference for all analyses
207 in this subsection.

208   We begin by analyzing the MHT and AHT/OHT partitioning estimated using two
209 additional satellite-derived observational estimates of TOA radiation (see Supporting In-
210 formation for details): the unadjusted CERES single scanner footprint (SSF) data and
211 the ERBE satellite data which spans the 1984-1990 (left panels of Fig. 2 bordered by
212 the black box). In these three panels, the choice of TOA radiation product alters the cal-
213 culated observational MHT (solid black line) whereas the AHT is unchanged between

214 panels (ERA5 is used in each). Because the observational OHT is calculated from the
215 difference of MHT and AHT, the observational OHT estimate (solid blue line) also varies
216 between panels. Observational MHT calculated from the three different TOA radiation
217 products is consistently larger than the CMIP-mean in both hemispheres. Model biases
218 in MHT are largest when the CERES SSF product is used (Fig. 2E) and smallest when
219 the ERBE product is used (Fig. 2C). The CMIP-mean OHT is biased low compared to
220 that derived from all three TOA radiation datasets with largest magnitude biases when
221 CERES SSF is used, especially in the SH. Model biases in AHT/OHT partitioning are
222 insensitive to observational TOA radiation data set used which give a consistent estimate
223 of MHT despite their substantial (≈ 5 W m^{-2} = 2.5 PW globally integrated) differences
224 in global mean TOA radiative balance associated with absolute calibration uncertainty
225 (Loeb et al., 2009).

226 We next analyze the sensitivity of our results to the choice of atmospheric reanal-
227 ysis used to calculate the AHT (Fig. 2 panels A, B, D, F and H). In these five panels,
228 the MHT is identical (calculated using the CERES EBAF product) whereas the AHT
229 is calculated from the ERA5, ERA-interim, NCEP, MERRA2, and JRA reanalyses. Since
230 OHT is calculated from the residual of MHT and AHT, the OHT difference between the
231 three panels are equal and opposite to the the inter-panel differences in AHT. The CMIP-
232 mean bias toward too much poleward AHT and too little poleward OHT is apparent us-
233 ing all five observational estimates of AHT. Poleward AHT is largest when using ERA5
234 followed closely by JRA, MERRA2 and then ERA interim, whereas using NCEP pro-
235 duces the smallest poleward AHT with the most notable difference near the peak in the
236 SH at 40°S. Therefore, model biases in the AHT-OHT partitioning are smallest using
237 ERA5 and largest using NCEP. These results suggest that the sign and spatial struc-
238 ture of model biases in MHT partitioning are consistent across atmospheric reanalysis
239 datasets, whereas the magnitude of the bias depends on the reanalyses product used. Dif-
240 ferences in AHT calculated between the different reanalyses are not impacted by differ-
241 ences in the spatial resolution (see analysis and Fig. S2 in the Supporting Information)
242 as even the coarsest product (NCEP) resolves the spatial scales responsible for the vast
243 majority of AHT.

244 Finally, we evaluate whether heat storage due to the transient response to anthro-
245 pogenic forcing impacts our observational estimates of OHT. The Earth is not in equi-
246 librium but, rather, is accumulating energy at an average rate of 0.7 W m^{-2} globally (John-
247 son et al., 2016). The vast majority of this energy accumulation is stored in the ocean
248 (Von Schuckmann et al., 2016) and it is possible that the spatial structure of this energy
249 storage projects onto our diagnoses of observational OHT for the following reason: ob-
250 served 'implied' OHT is calculated from the spatial integral of inferred surface heat fluxes
251 (TOA radiation plus AHT convergence) and the latter is balanced by the sum of OHT
252 divergence and ocean heat storage in a transient system. We diagnose the impact of ob-
253 served ocean heat storage on the implied OHT (OHT$_{\text{STORAGE}}$) from the trend in ocean
254 heat content, derived from UK Hadley Center EN4 objective ocean analysis (Good et
255 al., 2013) over the CERES period (see Supporting Information for details). OHT$_{\text{STORAGE}}$
256 is removed from the 'implied' OHT to estimate the 'true' OHT (solid teal line in Fig.
257 1F) that must be transported laterally in the ocean to close the ocean energy budget.
258 OHT$_{\text{STORAGE}}$ is very small (< 0.1 PW in magnitude) and, thus, the diagnosed 'true'
259 OHT is visually indistinguishable from the observational 'implied' OHT (solid blue line
260 in Fig. 1F). The global mean ocean heat uptake of 0.7 W m^{-2} translates to 0.4 PW of
261 global energy input to the ocean but the implied OHT of ocean heat storage is signif-
262 icantly smaller in magnitudes due to ocean heat uptake being more globally uniform than
263 regionally isolated. The negligible impact of ocean heat storage on 'implied' OHT over
264 the historical period is consistent with the small (< 0.1 PW) differences between OHT
265 in the ensemble mean of historical CMIP5 simulations averaged over the 2000-2018 time
266 period as compared the pre-industrial control simulations using the same models (Sup-
267 porting Information Fig. S3).

268 Collectively, these results suggest that the sign of model biases in AHT-OHT par-
269 titioning is robust to different observational products (satellite TOA radiation and at-
270 mospheric reanalysis) used to partition MHT. Additionally, the spatial pattern of tran-
271 sient heat uptake by the ocean makes a negligible impact on estimated OHT. However,
272 the magnitude of the model bias in AHT-OHT partitioning does vary with observational
273 datasets used. In this regard, the use of CERES EBAF and ERA5 data for our primary
274 analysis (Fig. 1) is a conservative estimate of model biases in AHT-OHT partitioning
275 (a smaller OHT bias is found only when using the combination of ERBE and ERA5 prod-
276 ucts).

4 Biases in energy input to the atmosphere and ocean and inferred AHT and OHT biases

279 Here we evaluate potential causes of the persistent model biases in AHT and OHT
280 in terms of model biases in the spatial structure of energy input into the ocean and at-
281 mosphere. Starting in the ocean, energy conservation demands that OHT across a lat-
282 itude band balances the net surface heat flux *out* of the ocean (-SHF by our sign con-
283 vention) integrated over the polar cap bounded by that latitude, which from Eq. 1 is rep-
284 resented by:

$$\text{OHT}(\Theta) = 2\pi a^2 \int_{\Theta}^{90} (-\text{SHF}^*)\, cos(\theta) d\theta. \tag{2}$$

285 SHF is equal to the net downward surface radiation (RAD_{SURF}) into the ocean minus
286 the upward turbulent energy fluxes of sensible (SENS) and latent heat (L_vE):

$$\text{SHF} = \text{RAD}_{\text{SURF}} - \text{SENS} - \text{L}_v\text{E}. \tag{3}$$

287 Substitution of Eq. (3) into Eq. (2) allows the OHT to be decomposed into the implied
288 transports of each term contributing to SHF:

$$\text{OHT} = \text{OHT}_{\text{RAD,SURF}} + \text{OHT}_{\text{SENS}} + \text{OHT}_{\text{E}}, \tag{4}$$

289 where, for example, the OHT implied by evaporation (OHT_{E}) is:

$$\text{OHT}(\Theta)_{\text{E}} = 2\pi a^2 \int_{\Theta}^{90} \text{L}_v\text{E}^* cos(\theta) d\theta, \tag{5}$$

290 where, as in Eq. 1 and 2, the * indicates that the global (ocean domain) mean has been
291 removed from the term. Because SENS* is small compared to the other terms (Fig. 3C)
292 and RAD_{SURF} is dominated by solar input to the surface (Supporting Information Figs.
293 S5E,F), the predominant energy balance in this framework can be summarized as fol-
294 lows: the magnitude of OHT (black line in Fig. 3D) is governed by the imbalance be-
295 tween excess (relative to the global mean) solar radiation entering the tropical ocean (or-
296 ange line) and excess evaporative loss (green). Perfect local compensation between sur-
297 face solar input and evaporation implies zero OHT whereas weaker evaporative loss de-
298 mands a larger fraction of solar input be realized as OHT. We use this framework to un-
299 derstand model biases in OHT in terms of biases in the meridional structure of terms
300 contributing to SHF.

301 The latitudinal structure of CMIP-mean L_vE, SENS and SURF_{RAD} over the ocean
302 domain is compared to observational estimates of the same quantities with L_vE and SENS
303 taken from the WHOI Objectively Analyzed (OA) Air-Sea Flux product (Yu et al., 2004)
304 and SURF_{RAD} estimates from the CERES EBAF surface product (Kato & Coauthors,

305 2018) in Fig. 3C. Evaporation is biased high in models (relative to the observational es-
306 timate) at all latitudes except the Arctic (Supporting Information Fig. S4). Evapora-
307 tion biases are largest (> 20 W m^{-2}) in the subtropics of both hemispheres and are much
308 smaller in the high latitudes. These evaporation biases manifest as enhanced subtrop-
309 ical ocean energy loss by E* in the models (cf. the dashed and solid green lines in Fig.
310 3C) and an implied model bias toward too little (by approximately 0.4 PW) poleward
311 OHT due to evaporation in each hemisphere (OHT$_{\text{E}}$, green line in Fig. 3D). Thus, evap-
312 oration biases alone explain the majority of the model bias in OHT identified in Section
313 3 (compare green and dashed black lines in Fig. 3D).

314 The observational RAD$^*_{\text{SURF}}$ has a stronger equator-to-pole gradient than that in
315 climate models (cf. the solid and dashed orange lines in Fig. 3C) especially in the SH.
316 Model biases in RAD$^*_{\text{SURF}}$ are associated with larger than observed downwelling solar
317 radiation into the extratropical Southern Ocean (Supporting Information Fig. S5E) due
318 to clouds that are optically thinner than observed (Donohoe & Battisti, 2012). As a re-
319 sult, observed poleward OHT$_{\text{RAD,SURF}}$ is larger than that in models with larger mag-
320 nitude (0.4 PW) biases in the SH. The model biases in OHT$_{\text{RAD,SURF}}$ mirror the im-
321 pact of TOA radiation biases on MHT (left panels of Figure 1) including the partition-
322 ing between shortwave and longwave biases within each hemisphere, suggesting that model
323 biases in MHT and OHT in the SH are due to biases in shortwave absorption whereas
324 those in the NH are due to biases in OLR and net surface longwave (Supporting Infor-
325 mation Figs. S5B,F).

326 The sum of model biases in OHT$_{\text{E}}$, OHT$_{\text{RAD,SURF}}$ and OHT$_{\text{SENS}}$ (solid black line
327 in Fig. 3D) finds that models would have weaker than observed poleward OHT of 0.6
328 PW in the NH and 0.8 PW in the SH based on biases in energy input to the ocean. This
329 overall inferred OHT bias is primarily due to a nearly hemispherically mirror-imaged bias
330 in OHT$_{\text{E}}$ which is enhanced by poleward OHT$_{\text{RAD,SURF}}$ in the SH. The bias in OHT
331 inferred from surface flux biases matches the spatial structure but exceeds in magnitude
332 the OHT biases calculated in Section 3 from TOA radiation and atmospheric reanaly-
333 sis (dashed black line in Fig. 3D). These two calculations of model OHT biases do not
334 have to match as they use different conceptual approaches and rely on completely in-
335 dependent observational climate fields. Nonetheless, the consistency of the sign, spatial
336 pattern, and magnitude of the OHT biases calculated using the two different approaches
337 suggest that the model biases in surface energy fluxes are large enough to account for
338 the AHT-OHT partitioning biases inferred from the residual TOA radiation and AHT
339 estimates.

340 We use a similar calculation of the model biases in implied AHT from the spatial
341 structure of energy input to the atmosphere to compute an alternative estimate of AHT
342 biases to those calculated in Section 3. The AHT analog to Eq. 4 is:

$$\text{AHT} = \text{AHT}_{\text{RAD,ATMOS}} + \text{AHT}_{\text{SENS}} + \text{AHT}_{\text{E}}, \qquad (6)$$

343 where the atmospheric analog to Eq. 5 for the AHT due to evaporation (AHT$_{\text{E}}$) is:

$$\text{AHT}(\Theta)_E = 2\pi a^2 \int_{\Theta}^{90} -\text{L}_\text{v}\text{E}^* cos(\theta)d\theta. \qquad (7)$$

344 The spatial integral is over a global (land plus ocean) domain. Here RAD$_{\text{ATMOS}}$ is the
345 net radiative heating of the atmospheric column which is equivalent to the net radiation
346 at TOA minus RAD$_{\text{SURF}}$. Fajber et al. (2023) demonstrated that poleward AHT is pri-
347 marily determined by evaporation (AHT $\approx$ AHT$_{\text{E}}$) because L$_\text{v}$E* dominates the spa-
348 tial structure of energy input to the atmosphere. We note that L$_\text{v}$E* spatially integrated
349 over the ocean domain has opposing impacts on AHT$_{\text{E}}$ versus OHT$_{\text{E}}$ (and likewise for
350 SENS* and AHT$_{\text{SENS}}$ versus OHT$_{\text{SENS}}$). This arises because excess evaporation over the

low latitudes ($E^* > 0$) adds energy to the atmosphere to enhance the demand for poleward AHT at the expense of removing energy from the low-latitude ocean to reduce the demand for poleward OHT.

To more clearly see the compensation between biases in AHT-OHT due to model biases in $L_v E^*$ (and SENS*) over the ocean domain, we take the following approach to compare models and observations of AHT via Eqs. 6 and 7. First, AHT$_E$ and AHT$_{SENS}$ are calculated from the observational WHOI OA evaporation and sensible heat flux data *over the ocean domain only*, and are compared to analogous model calculations over the ocean domain. Then, the contribution of turbulent energy fluxes over land to the combined AHT$_E$ and AHT$_{SENS}$ is estimated from the CERES EBAF net surface radiation spatially integrated over land. This approach assumes that (via surface energy balance) surface radiative gain is balanced by turbulent loss. These calculations are compared to analogous calculations in the models. Finally, AHT$_{RAD,ATMOS}$ is calculated from the CERES EBAF TOA and surface data *over the global domain* and is compared to the analogous global domain calculation in models (orange lines in Fig. 3A,B). This strategy circumvents the lack of reliable observational estimates of turbulent energy fluxes over land – instead inferring them from a like-with-like observational-to-model comparison of surface radiation over land and assuming that RAD$_{SURF}$ is balanced by upward turbulent fluxes from the land to the atmosphere (the latter assumption has been validated in models).

Model biases in AHT$_E$ compose the vast majority of AHT biases diagnosed from Eq. 6 (cf. the green and solid black lines in Fig. 3B) and suggest that the stronger than observed poleward AHT in models is driven by an enhanced equator-to-pole gradient in evaporation. Model RAD$^*_{ATMOS}$ is more negative in the deep tropics as compared to observations (due to stronger longwave cooling in the models– Supporting Information Fig. S5) which contributes to smaller AHT$_{RAD,ATMOS}$ export from the tropics in the models that generally opposes the low latitude biases in AHT$_E$ (orange line in Fig. 3B). Interestingly, shortwave absorption in the atmosphere is biased low in the models, which reduces the demand for poleward AHT by nearly 0.4 PW in both hemispheres (red line in Supporting Information Fig. S5D). However, this model deficit in atmospheric heating of the tropics is nearly compensated for by weaker than observed longwave cooling of the atmosphere such that there is almost no bias in AHT$_{RAD,ATMOS}$ at the equator-to-pole scale. Turbulent energy fluxes over the land inferred from net surface radiation are nearly identical in models and observations and make a negligible impact on AHT biases (cf. purple dashed and solid lines in Fig. 3C,D).

These calculations demonstrate that the model biases in the partitioning of poleward heat transport between AHT and OHT that were inferred in Section 3 are consistent (in sign, spatial structure, and magnitude) with the model biases in energy input into the atmosphere and ocean by radiative fluxes and turbulent exchange between the atmosphere and ocean. Stronger than observed evaporation in the models contributes to enhanced poleward AHT at the expense of reduced OHT that is nearly hemispherically symmetric whereas radiative biases due to thinner than observed clouds in the extratropical Southern Ocean results in too weak poleward MHT that is primarily manifested in the surface energy budget and implied OHT bias.

5 Summary and discussion

Coupled climate models have too little poleward OHT in both hemispheres and too much AHT in the NH, compared to observational estimates. These model biases are remarkably consistent across three generations of coupled model ensembles (CMIP3, CMIP5, and CMIP6) and across different sets of observational TOA radiation and atmospheric reanalysis data. These conclusions are not impacted by observed transient energy accumulation in the ocean.

The method used here to balance the mass budget of the atmospheric reanalysis differs from that used in the work of Trenberth & Stepaniak (2004) and M. et al. (2017). Specifically, we implicitly assume zero net atmospheric mass flux through a given latitude circle whereas other works adjust the mass flux to balance the polar cap spatial integral of the surface pressure tendency and evaporation minus precipitation. Our choice stems from defining the energy budget with respect to a fixed mass of atmosphere (Donohoe & Battisti, 2013; Liang et al., 2018). The AHT associated with the mass flux due to evaporation minus precipitation is primarily compensated for a return flow of mass and energy in the ocean and requires a consistent treatment of the energy fluxes through the atmosphere, surface and ocean (M. et al., 2017) that depends on the choice of zero point energy (e.g., the units used for temperature). Physically, a poleward (water) mass flux in the atmosphere is balanced by the mass flux of precipitation minus evaporation and an equivalent equatorward mass flux in the ocean. The energy flux of each of these mass fluxes is the product of mass flux and mean energy of the fluid, has a minimal net (AHT+OHT) poleward energy transport but is of order 0.2 PW in magnitude for each the compensating AHT and OHT. The standard definition of SHF in climate models does not include the sensible heat of this net (water) mass flux across the air/sea interface and we believe including this term would create an inconsistency between the model derived and observationally inferred OHT. Our interpretation is supported by the near equivalence of the AHT calculated in CESM via the "observational" and "model" partitioning calculations using our method of calculating AHT from reanalysis data whereas including the net mass flux of water in the AHT creates a substantial mismatch between the two calculations (not shown). We emphasize that all choices made here were aimed at creating a consistent way to compare observational and model MHT and AHT-OHT partitioning despite the different climate fields that go into each calculation.

This work focused on model biases in the vertical zonal and time integral of atmospheric moist static energy fluxes that comprise AHT without regard for biases in the underlying atmospheric circulations and associated temperature and humidity structures of the atmosphere. Donohoe et al. (2020) demonstrated that model biases in poleward AHT primarily result from larger than observed dry (sensible) heat transport by transient eddies in the mid-latitudes of both hemisphere (their Fig. 4D) and in the NH smaller than observed dry heat transport by stationary eddies; the moisture (latent heat) transport has negligible biases. Model biases in evaporation are expected to be manifested as biases in both moist and dry AHT because dry AHT is set by the spatial pattern of condensational heating of the atmosphere which represents the portion of AHT_E that is not transported poleward as latent heat (Fajber et al., 2023); while spatial patterns of evaporation directly demand poleward moist AHT, the energy input to the atmosphere via evaporation is handed off to dry AHT where precipitation forms and the atmosphere is heated condensationally. Therefore, our finding that model biases toward too much AHT result from stronger than observed evaporation is consistent with the finding that excess poleward AHT in the models is expressed as a bias toward too much dry heat transport.

Remarkably, the model OHT bias inferred from observational estimates from satellite TOA radiation and atmospheric reanalyses is in descent agreement with model biases in the energy exchange between the ocean and atmosphere calculated from independent observational estimates of surface heat fluxes. The latter bias is due primarily to stronger than observed low-latitude evaporation in the models. We note that the community has been reluctant to diagnose OHT from the observed surface energy balance because of uncertainty in the turbulent energy fluxes. Yet, our analysis paints a consistent picture of the model biases in turbulent energy fluxes – whether these are inferred from the residual of TOA radiation and AHT or from bulk formula. We also note that observational estimates of global mean evaporation and its equator-to-pole gradient vary substantially (Stephens et al., 2012) with reanalysis products generally having more evaporation than the bulk formula based estimates such as WHOI OA flux (Yu et al., 2004)

and SEAFLUX (Curry et al., 2004). We chose to use WHOI OA flux for the analysis in Section 4 because the bulk formula in this product are optimized to match buoy observations – making it the most observationally constrained estimate of evaporation. Additionally, the global constraint of evaporation balancing precipitation is nearly satisfied from the combination of the WHOI OA FLUX evaporation over the ocean (62.8 W m^{-2} contribution to global mean) plus the ERA5 reanalysis evaporation over land (12.9 W m^{-2} for a global total evaporation of 75.7 W m^{-2}) nearly balancing the best observational estimate of global mean precipitation (77.9 W m^{-2}) from the NOAA GPCP (Adler et al., 2018). The lack of closure of the observed global mean surface energy budget suggests that observational surface radiation and/or turbulent energy fluxes are poorly constrained and one hypothesized solution is that both global mean evaporation and precipitation are substantially underestimated (Stephens et al., 2012). Our analysis circumvents this debate by removing global mean quantities, showing that the equator-to-pole gradient of surface energy fluxes is consistent with that inferred from TOA radiation and AHT divergence. This suggests that the meridional structure of surface energy fluxes constrained by TOA radiation and AHT could be used in conjunction with global mean imbalances to give an additional constraint for reconciling which terms in the observed surface energy budget are most uncertain and/or biased.

6 Open Research

All underlying observational data sets are publicly available. The CMIP data analyzed in this study can be found in the Earth System Grid392 Federation (ESGF) repository at `https://esgf-node.llnl.gov/projects/esgf-llnl`. Observational calculations of AHT from the vertical integral of 6 hourly reanalysis data (MERRA, ERA5, NCEP and JRA) are available at `https://atmos.uw.edu/~aaron/cmip_AHT_partition/`.
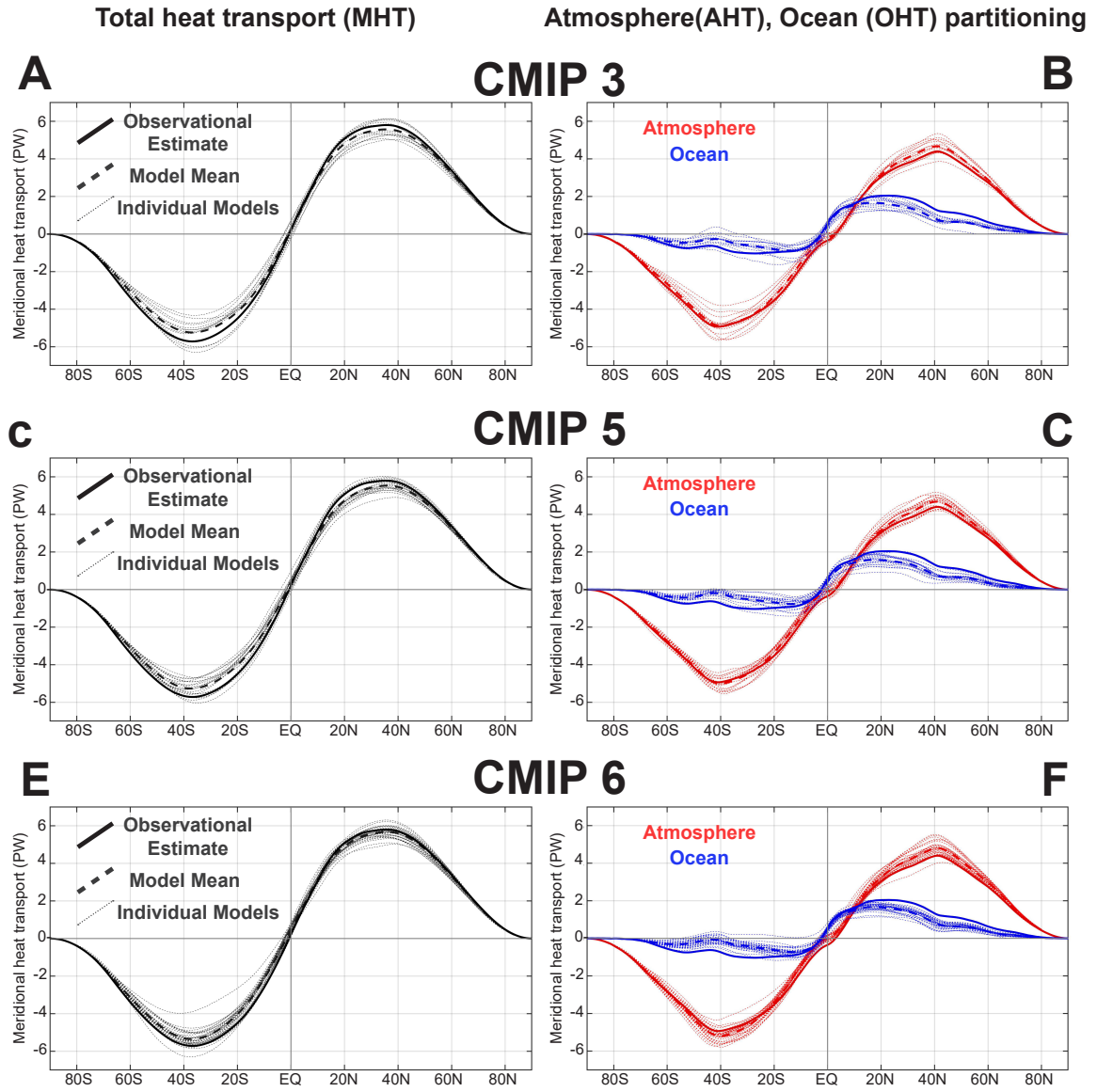
Figure 1. Observational and model (left panels) total meridional heat transport (MHT) and (right panels) its partitioning between the atmosphere (AHT, red) and ocean (OHT, blue). Results from the CMIP3, CMIP5, and CMIP6 models are shown in the top, middle and bottom panels respectively. The observational estimates are shown by the heavy solid line, individual coupled models are shown by the dotted lines and the model ensemble mean is shown by the heavy dashed line.
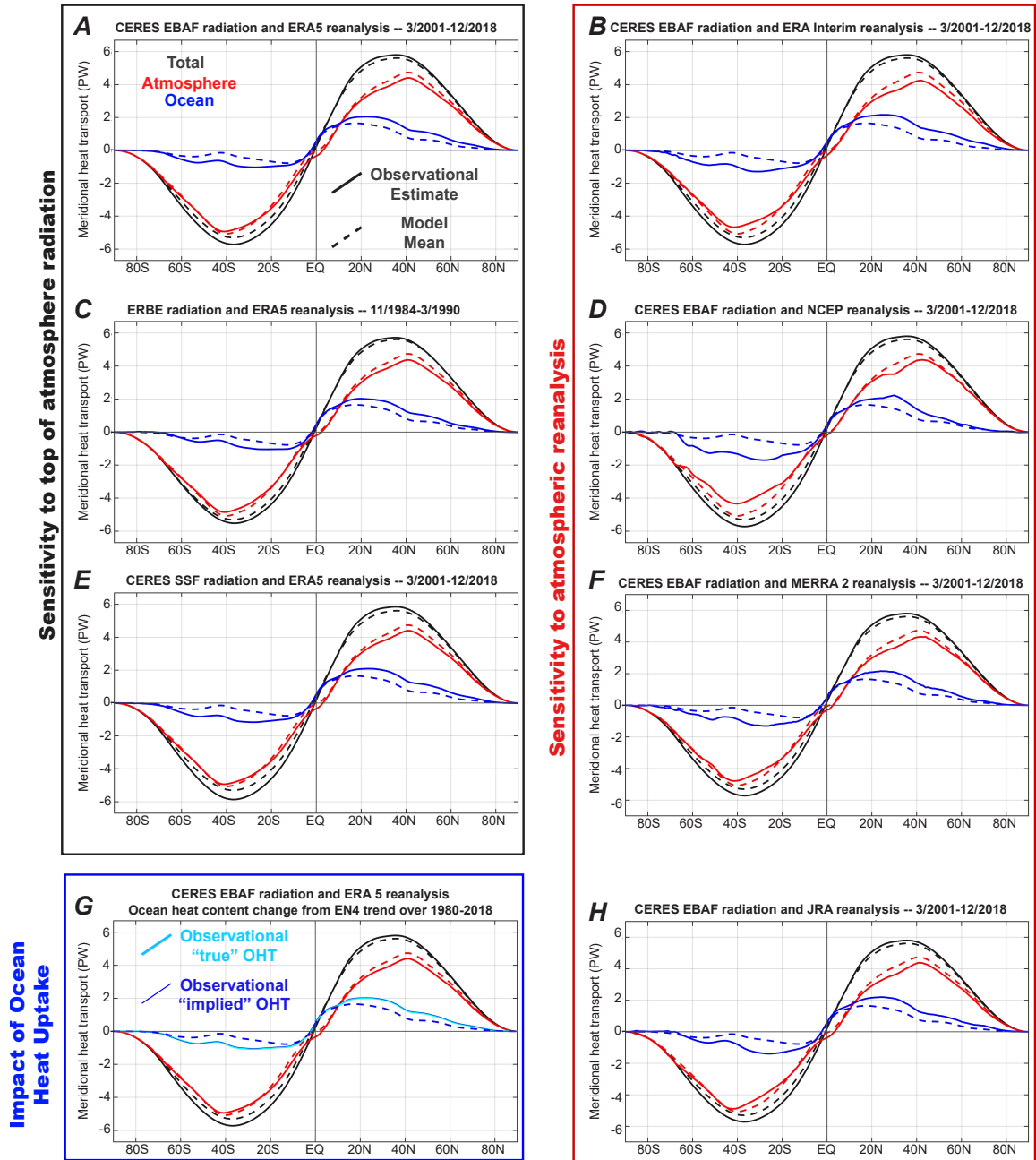
Figure 2. Comparison of MHT, OHT and AHT in models and observations using eight different observational estimates of MHT (black solid), AHT (red), and OHT (blue). The left panels show the sensitivity of the transports to TOA radiation product used with CERES EBAF on the top panel, ERBE in the second panel, and the unadjusted CERES SSF on the bottom and with the ERA5 AHT estimate across all panels. The right panels show the observational transports calculated using CERES EBAF TOA radiation in all panels but using different atmospheric reanalysis products in each panel: (B) ERA Interim; (D) NCEP; (F) MERRA2 and; (H) JRA. Panel (G) shows the impact of observed spatial patterns in ocean heat storage on implied OHT using EN4 ocean heat content changes over 2000-2018. The model mean is the average over all models in CMIP3, CMIP5, and CMIP6 (CMIP-mean).
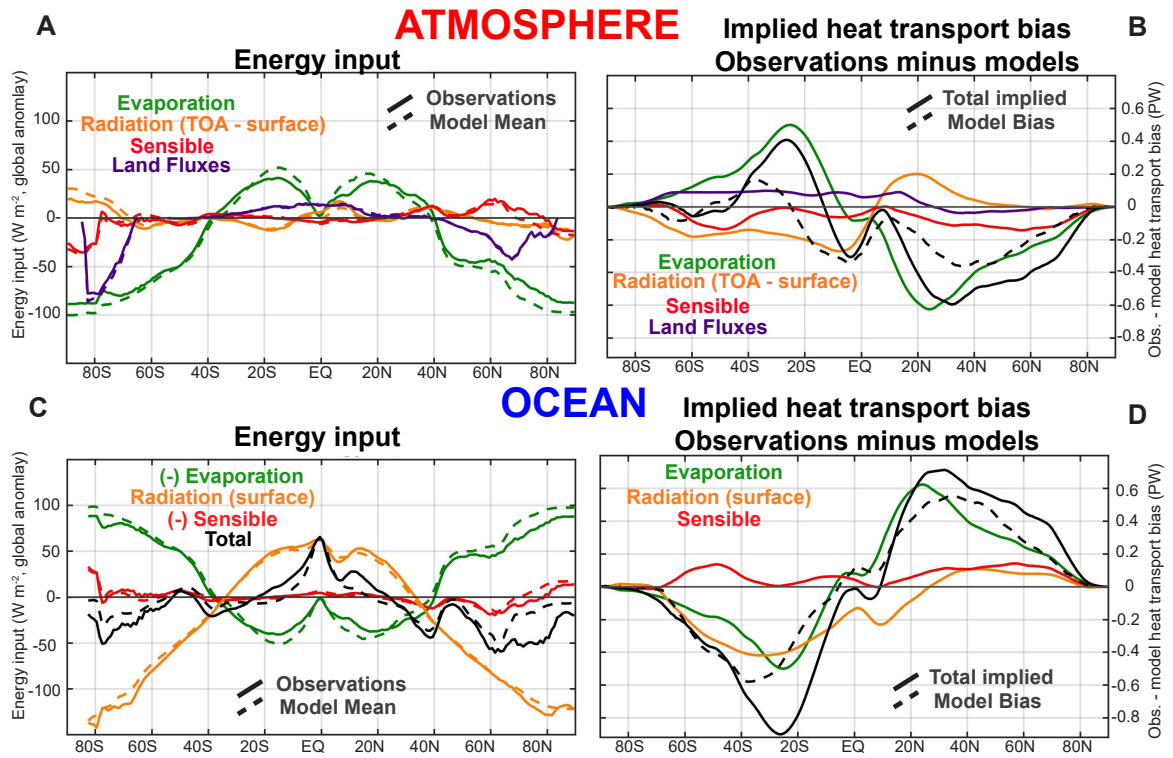
Figure 3. Model and observational estimates of the energy input into the atmosphere and ocean and the implied AHT and OHT biases resulting from each input. (A) Global anomaly energy input into the atmosphere in models (dashed) and observations (solid). See text for definition of terms. (B) Implied AHT bias (observations minus models) due to each energy input. The solid black line shows the sum of all terms. The dashed black line shows the bias in heat transport inferred from CERES and ERA5 data. (C) As in A but for the energy input to the ocean. (D) As in B but for the implied OHT bias.

References

Adler, R., Sapiano, M., Huffman, G., Wang, J., Gu, G., Bolvin, D., . . . Shin, D. (2018). The global precipitation climatology project (GPCP) monthly analysis (new version 2.3) and a review of 2017 global precipitation. *Atmosphere*, *9*(4). doi: 10.3390/atmos9040138

Cardinale, C., Rose, B., Lang, A., & Donohoe, A. (2020). Stratospheric and tropospheric flux contributions to the polar cap energy budgets. *J. Climate*, *34*(11), 4261-4278.

Curry, J., Bentamy, A., Bourassa, M., Bourras, D., Bradley, E. F., Brunke, M., . . . Zeng, X. (2004). Seaflux. *Bull. Amer. Meteor. Soc.*, 490-424. doi: 10.1175/BAMS-85-3-409

Donohoe, A., Armour, K., Roe, G., & Battisti, D. (2020). The partitioning of meridional heat transport from the Last Glacial Maximum to CO_2 quadrupling in coupled climate models. *J. Climate*, *33*(10), 4141-4165.

Donohoe, A., & Battisti, D. (2011). Atmospheric and surface contributions to planetary albedo. *J. Climate*, *24*(16), 4401-4417.

Donohoe, A., & Battisti, D. (2012). What determines meridional heat transport in climate models? *J. Climate*, *25*, 3832-3850.

Donohoe, A., & Battisti, D. (2013). The seasonal cycle of atmospheric heating and temperature. *J. Climate*, *26*(14), 4962-4980.

Enderton, D., & Marshall, J. (2009). Controls on the total dynamical heat transport of the atmosphere and oceans. *J. Atmos. Sci.*, *66*, 1593-1611.

Fajber, R., Donohoe, A., Ragen, S., Armour, K., & Kushner, P. (2023). The hydrologic cycle drive atmospheric heat transport. *Proc. Nat. Acad. Sci.*, *120*(25), e2217202120. doi: 10.1073/pnas.2217202120

Flato, G., Marotzke, J., Abiodun, B., Braconnot, P., Chou, S., Collins, W., . . . Rummukainen, M. (2013). Evaluation of climate models [Book Section]. In T. Stocker et al. (Eds.), *Climate change 2013: The physical science basis. contribution of working group i to the fifth assessment report of the intergovernmental panel on climate change* (p. 659Â–740). Cambridge University Press. doi: 10.1017/CBO9781107415324.018

Good, S. A., Martin, M., & Rayner, N. (2013). En4: quality controlled ocean temperature and salinity profiles and monthly objective analyses with uncertainty estimates. *J. Geophys. Res.-Oceans*, *118*, 6704-6716.

Hersbach, H. B. B., Berrisford, P., Hirahara, S., Horanyi, A., Munoz?Sabater, J., Nicolas, J., & Peubey, C. (2020). The era5 global reanalysis. *Quart. J. Roy. Meteor. Soc.*. doi: 10.1002/qj.3803

Holland, M. M., Bitz, C., & Tremblay, B. (2006). Future abrupt reductions in the summer arctic sea ice. *Geophys. Res. Lett.*, *33*(23). doi: 10.1029/2006GL028024

Johnson, G., Lyman, J., & Loeb, N. (2016). Improving estimates of Earth's energy imbalance. *Nat. Clim. Chang.*, *6*(7), 639-640.

Kato, S., & Coauthors. (2018). Surface irradiances of edition 4.0 clouds and the Earth's radiant energy system (CERES) energy balanced and filled (EBAF) data product. *J. Climate*, *31*(11), 4501-4527.

Liang, M., Czaja, A., Graversen, R., & Tailleux, R. (2018). Poleward energy transport: is the standard definition physically relevant at all time scales? *Climate Dyn.*, *50*, 1785-1797.

Loeb, N. G., & Coauthors. (2018). Clouds and the Earth's radiant energy system (CERES) energy balanced and filled (EBAF) top-of-atmosphere (TOA) edition 4.0 data product. *J. Climate*, *31*(2), 895-918.

Loeb, N. G., Wielicki, B. A., Doelling, D. R., Smith, G. L., Keyes, D. F., Kato, S., . . . Wong, T. (2009). Towards optimal closure of the Earth's top-of-atmosphere radiation budget. *J. Climate*, *22*, 748-766.

Lucarini, V., & Ragone, F. (2011). Energetics of IPCC4AR4 climate models: energy balance and meridional enthalpy transports. *Rev. Geophys.*, *49*, RG1001.

M., M., Haimberger, L., Edwards, J., & Hyder, P. (2017). Toward consistent diagnostics of the coupled atmosphere and ocean energy budgets. *J. Climate*, *22*(30), 9225-9246.

Mayer, J., Mayer, M., & Haimberger, L. (2021). Consistency and homogeneity of atmopsheric energy, moisture and mass budgets in ERA5. *J. Climate*, *34*(10), 3955-3974.

Oort, A., & Haar, T. V. (1976). On the observed annual cycle in the ocean–atmosphere heat balance over the Northern Hemisphere. *J. Phys. Oceanogr.*, *6*, 781-800.

Pierrehumbert, R. (2010). *Principles of planetary change.* Cambridge University Press.

Seager, R., Battisti, D., Yin, J., Naik, N., Gordon, N., Clement, A., & Cane, M. (2002). Is the gulf stream responsible for europe's mild winters? *Quart. J. Roy. Meteor. Soc.*, *128*, 2563-86.

Stephens, G., Li, J., Wild, M., Clayson, C., Loeb, N., Kato, S., . . . Andrews, T. (2012). An update on Earth's energy balance in light of the latest global observations. *Nat. Geo. Sci.*, *5*, 691-696. doi: 10.1038/ngeo15802

Stone, P. (1978). Constraints on dynamical transports of energy on a spherical planet. *Dynam. Atmos. Oceans*, *2*, 123-139.

Trenberth, K. E., & Caron, J. M. (2001). Estimates of meridional atmosphere and ocean heat transports. *J. Climate*, *14*, 3433-3443.

Trenberth, K. E., Fasullo, J. T., & Kiehl, J. (2009). Earth's global energy budget. *Bull. Amer. Meteor. Soc.*, *90*(3), 311-324.

Trenberth, K. E., & Stepaniak, D. P. (2003). Co-variability of components of poleward atmospheric energy transports on seasonal and interannual timescales. *J. Climate*, *16*, 3691-3705.

Trenberth, K. E., & Stepaniak, D. P. (2004). The flow of energy through the earth's climate system. *Quart. J. Roy. Meteor. Soc.*, *130*, 2677-2701.

Vonder Haar, T., & Oort, A. (1973). New estimate of annual poleward energy transport by Northern Hemisphere oceans. *J. Phys. Oceanogr.*, *2*, 169-172.

Von Schuckmann, K., Palmer, M., Trenberth, K., Cazenave, A., Chambers, D., Champollion, N., . . . Wild, M. (2016). An imperative to monitor earth's energy imbalance. *Nat. Clim. Change.*, *6*, 138-144. doi: 10.1038/nclimate2876

Yu, L., Weller, R., & Sun, B. (2004). Improving latent and sensible heat flux estimates for the Atlantic Ocean (1988-1999) by a synthesis approach. *J. Climate*, *17*, 373-393.